Mechanism of Hook Formation in Ultra-low Carbon Steel based on Microscopy Analysis and Thermal-stress Modeling

Joydeep Sengupta
Postdoctoral Research Associate
&
Brian G. Thomas
Wilkins Professor
Department of Mechanical and Industrial Engineering
University of Illinois at Urbana-Champaign
Urbana, Illinois 61801, USA
Tel: 217-333-6919
Fax: 217-244-6534
Email: bgthomas@uiuc.edu

Ho-Jung Shin
Graduate Student
&
Seon-Hyo Kim
Professor
Department of Materials Science and Engineering
Pohang University of Science and Technology
Pohang, Kyungbuk 790-784, South Korea
Tel: 82-54-279-2815
Fax: 82-54-279-2399
Email: seonhyo@postech.ac.kr

Keywords: Continuous casting, Oscillation marks, Hooks, Ultra-low carbon steel, formation mechanism, Solidification microstructure, Electron microscopy, Finite Element models

INTRODUCTION

Periodic transverse depressions called "oscillation marks" are routinely observed on the surface of steel slabs manufactured by continuous casting processes[1-3]. Additionally, a distinctive sub-surface microstructural feature called a "hook"[2, 4, 5] often accompanies deep oscillation marks in steels with low (< 0.1%) carbon contents[4, 6]. **Figure 1** shows typical shapes and sizes of oscillation marks and hooks observed on specially-etched samples obtained from ultra-low (0.003% C) carbon steel slabs cast at POSCO Gwangyang Works, South Korea[7, 8]. Hooks can be classified as "curved" (**Figure 1(a)**) if they angle steeply inwards from the surface or "straight" (**Figure 1(b)**) if they are shallow and lie just beneath and parallel to the surface[9]. Curved hooks reach deeper beneath the surface (1.42 mm *vs.* 0.48mm for straight hooks) and are accompanied by deeper oscillation marks (0.26 mm *vs.* 0.19 mm for straight hooks). Each hook has a central line, the "line of hook origin", which distinguishes the region inside the hook microstructure from the portion that solidified after liquid steel overflow.

Increasing severity of hooks and oscillation marks is associated with lower slab surface quality, owing to the entrapment of argon bubbles and alumina inclusions near the hook[10, 11], and the formation of transverse cracks near the roots of oscillation marks[1, 3, 6]. Transverse cracks initiate due to the coarser grain structure and embrittling precipitates often found in this region[3, 6]. In some cases, the entire slab surface must be ground or "scarfed" to remove these defects, resulting in higher cost and productivity loss[7].

The formation of hooks and oscillation marks is associated with vertical oscillation of the water-cooled copper mold, which significantly alters the local heat transfer, fluid flow and initial solidification in the meniscus region. The oscillation is required to facilitate smooth withdrawal of the solidifying steel shell from the mold by preventing the shell from sticking to the mold wall. This is aided by a "negative strip time" period during the cycle, when the mold moves downward faster than the casting speed. Oscillation also pumps molten flux into the gap formed between the shell and mold faces, where it acts as a lubricant. The flux is added as a powder to the top free surface of the liquid steel pool. It melts to create a continuous liquid flux layer that conforms to the steel surface contour and flow field, and provides thermal and chemical insulation to the liquid steel. In addition to the mold oscillation frequency and stroke, many different parameters affect oscillation mark formation, including the casting speed, superheat temperature difference, and liquid steel flow pattern in the mold.

Several studies focusing on low-, medium-, and high-carbon steels have been conducted in the past to explain hook and oscillation mark formation, which is crucial to optimizing casting conditions for surface quality. Most previous mechanisms are based on transient events occurring near the meniscus, which involve the following complex, inter-related phenomena illustrated in **Figure 1(c)**:

1. Pressure fluctuations in the liquid flux channel dynamically alter the meniscus shape.
2. The turbulent flow pattern in the mold cavity brings liquid to the meniscus region with varying amounts of superheat.
3. Heat is conducted from the solidification front to the mold through the steel shell and the interfacial gap, which consists of liquid and re-solidified layers of mold flux.
4. The meniscus region might solidify, depending on the local superheat of the liquid, the availability of nucleation sites, the ease of nucleation and growth, and alloy properties such as freezing range.
5. The mold or slag rim may interact with the shell during the negative strip period, especially if mold friction is large enough to generate significant axial stresses and deformation.
6. Changing temperature gradient cause thermal distortion of the shell tip, depending on the mechanical properties of the steel grade.

All of the above events are expected to alter the rate of solidification near the meniscus and ultimately dictate the shape and size of sub-surface hooks and oscillation marks**.**

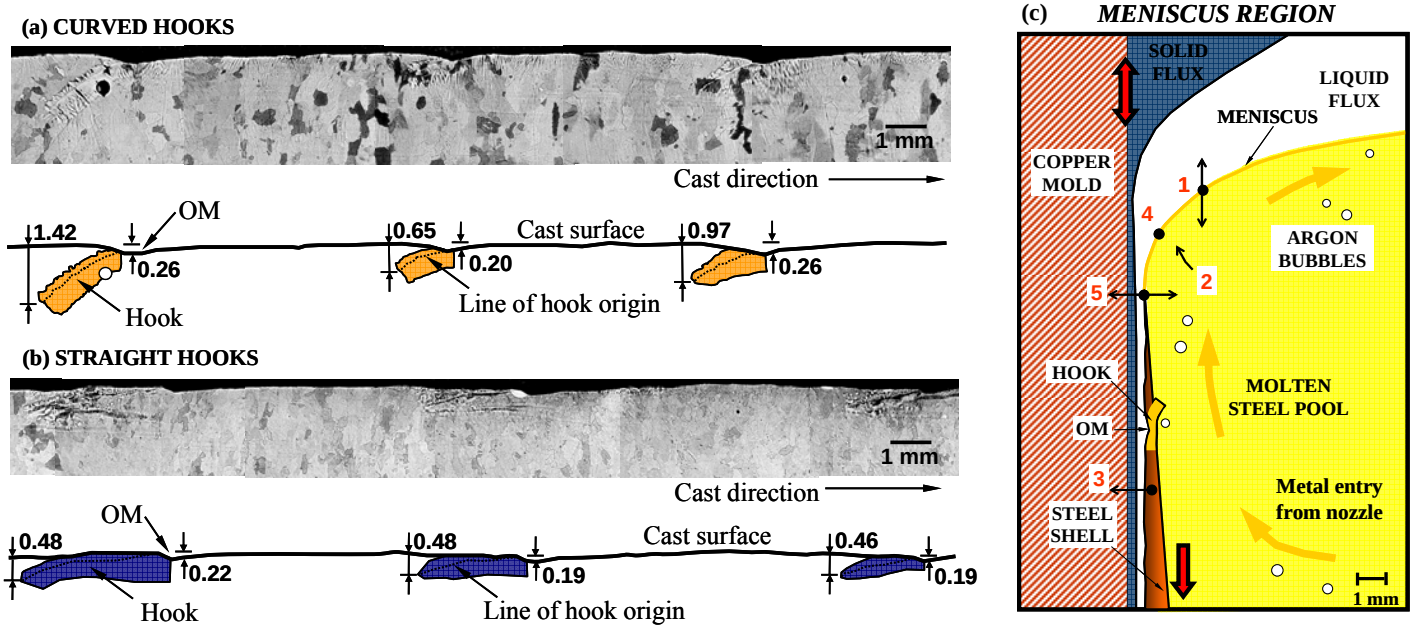

Figure 1 Three consecutive oscillation marks accompanied by (a) curved and (b) straight hooks observed on ultra-low carbon steel slabs[7, 8]; (c) complex phenomena occurring inside a continuous caster mold influence initial solidification in the meniscus region.

However, previous mechanisms offer conflicting explanations, and are often speculative and incomplete. For example, there is no agreement on when hooks form during the oscillation cycle or if they form by: (i) bending of the initial shell tip[12, 13], or (ii) freezing of the liquid steel meniscus[2, 4, 14-16]. The mechanisms for oscillation marks differ greatly from those proposed for surface depressions, which include: (i) healing of disjointed steel shell edges[17-19], and (ii) mechanical interaction between the mold and shell[20]; (iii) shell bending[12, 13], and (iv) thermal distortion[21] followed by liquid overflow over the shell tip and subsequent solidification.

A major impediment towards developing a robust understanding of initial solidification is the difficulty of observing hooks in cast samples. Special grade-specific etching reagents[4, 6, 22] are required to clearly reveal the initially solidified structure near the hook, prior to subsequent phase transformations. Previous efforts to observe hook features on slab samples have used either picric acid solution[3, 12] or Oberhoffer's reagent[3]. Although picric acid solution reveals the dendritic structure close to the oscillation mark, the hook is difficult to distinguish from the rest of the microstructure. On the other hand, Oberhoffer's reagent relies on the segregation of phosphorus, and can only reveal the linear profile of a hook but not the dendritic structure close to it. Thus, better etching reagents are needed. Furthermore, the relationship between the dendrite/hook microstructure and the final solidified grain structure has not been investigated in previous work. Scanning electron microscopy has also not been exploited to study hook formation.

Although microstructural analysis may provide important new information, but it cannot reveal the detailed steps that lead to the final microstructure and morphology. Therefore, fundamentally-based comprehensive mathematical models are required to predict events leading to hook and oscillation mark formation; but this is indeed a daunting task, requiring fully-coupled, transient thermal, fluid-flow, and stress analysis. Previous mathematical models to investigate initial solidification phenomena have oversimplified the

phenomena that lead to surface defect formation. The uncoupled thermal-mechanical model of shell tip bending by Schwerdtfeger and Sha[13] predicted inward tip bending up to ~0.6 mm, but the predicted oscillation mark depth did not decrease with higher mold oscillation frequencies and casting speeds, as observed in industry. The coupled thermal-stress model by Thomas and Zhu[21] predicted a shell tip deflection of ~1.65 mm for a liquid level drop of 20 mm for 1.2 s, which occurs rarely; so, this mechanism alone cannot explain the deep hooks (up to ~2 mm) observed in every one of a series of oscillation marks in an ultra-low carbon steel slab cast at POSCO (see **Figure 1(b)**).

To address the above issues, the present study was conducted to reveal new information about hook formation in ultra-low carbon steels. Both optical and scanning electron microscopy were performed to simultaneously distinguish the hook structure, the surrounding dendrite microstructure, the final grain structure, the grain orientations relative to the hook, and the local composition variations. In addition, a transient thermo-mechanical model was applied to compute temperature, stress development, and distortion of a steel shell during the initial stages of solidification by considering the effect of sudden metal level fluctuations at the meniscus. The model is based on a well-validated transient thermal-elastic-viscoplastic finite element code, CON2D[23], available at University of Illinois at Urbana-Champaign, and builds on previous work by Thomas and Zhu[21]. Finally, plant experiments were performed to quantify the effect of casting conditions on hook and oscillation mark severity in practice. The results obtained from these different sources reveal new insights into hook and oscillation mark formation during the initial stages of solidification in the meniscus region for ultra-low carbon steels.

EXPERIMENTAL METHODS

An experimental campaign was conducted on a conventional continuous slab caster, #2-1 at POSCO Gwangyang Works, South Korea. This caster features a standard 2-port submerged entry nozzle, a 230-mm thick parallel mold with a fully-adjustable, non-sinusoidal hydraulic oscillator, and electro-magnetic breaking forces to control fluid flow conditions in the liquid pool. **Table 1** summarizes the casting parameters employed to obtain the data and slab samples analyzed in this study. Further details are given elsewhere[7, 8].

Table I Casting parameters for slab samples

Micrograph analysis presented in:	Slab Width (*mm*)	Pour Temperature (^oC)	Casting Speed (*mm/s*)	Mold Oscillation Frequency (*Hz*)	Mold Oscillation Stroke (*mm*)
Figure 2 & 4	1300	1564	28.2	3.02	6.19
Figure 3	1300	1565	28.2	3.02	6.18
Figure 5	1960	~1565	~16.7	1.90	5.67

The composition of the ultra-low carbon steel grade used during the trials was: *Fe* with 0.003% *C*, 0.08% *Mn*, 0.005% *Si*, 0.015% *P*, 0.01% *S*, 0.01% *Cr*, 0.01% *Ni*, 0.01% *Cu*, 0.05% *Ti*, and 0.04% *Al*. The liquidus and solidus temperatures of this steel grade are 1533 ^{o}C and 1517 ^{o}C, respectively. The mold powder contained: 39.8% *CaO*, 36.33% SiO_2, 6.72% *F*, 5.97% Al_2O_3, 3.43% Na_2O, 0.84% *MgO*, 0.35% Li_2O, 0.34% Fe_2O_3, 0.18% TiO_2, 0.11% K_2O, 0.03% MnO_2, 1.97% *free C*, and 3.01% *total C*. Its melting temperature is 1145 ^{o}C and viscosity at 1300 ^{o}C is 2.62 Poise.

Samples (100-mm long and encompassing ~10-12 oscillation marks) were obtained near the surface of the narrow faces of 1300-mm wide slabs at five different distances between the wide faces. Sections through each sample were cut, mechanically ground and polished to ~0.25 μm. These were then etched by picric acid solution with additions of the cationic surface-active reagent or "surfactant"[24], zephiramine (Benzyldimethyl-n tetradecylammonium chloride) for ~1-1.5 hours. The etching reagent was identified by conducting an intensive experimental program at POSTECH to reveal the solidification microstructure and delineate the hook features in this difficult-to-etch steel grade with ultra-low alloy content under an optical microscope. Thus, micrographs (2-D vertical section views) were obtained of the hook [25] and oscillation mark structure at different locations down the narrow face. The shape of these structures does not vary much with distance along the slab perimeter. Near the corners of the slab, however, the hooks exhibit complex three-dimensional shapes.

The distribution of crystallographic orientation in the microstructure near the hook region was analyzed by the electron back scattering diffraction (EBSD) method using a JEOL JSM-7000F® field emission analytical scanning electron microscope. The microscope was equipped with a HKL Technology® EBSD system with a high resolution (up to 1.2 nm for a 30 kV accelerating voltage) detector that allowed accurate analysis of Kikuchi patterns over an area of 300 μm x 400 μm in steps of 2 μm. The samples were first electro-polished by 95% acetic acid-5% perchloric acid solution with a current of 0.2 A for 60 s. The data obtained from EBSD was analyzed using HKL Technology Channel 5® suite of programs, which can display subtle changes in orientation along a line running across grains or sub-grains. The hook region of samples from a 1960-mm wide slab was also subjected to elemental analysis by the energy dispersive x-ray spectroscopy (EDXS) method using a JEOL JSM-59® scanning electron microscope.

Metallographic assessment of hook shapes

Figure 2(a) shows a typical "curved" hook adjacent to an oscillation mark in one of the slab samples, shown in **Figure 1(b)**. Each hook has a curved line determined to be the "line of hook origin", which indicates the shape of the meniscus after it solidified. Groups of dendrites growing both away and towards the mold surface from this line can be clearly distinguished, owing to the marked improvement of the current etching method over those used in previous studies[3, 12]. The characteristic features (*e.g.* length, depth and thickness) of the hook can be easily measured from the micrograph. Traces of entrapped bubbles and inclusion particles were often found in the vicinity of curved hooks, such as can be seen in this figure. The perpendicular distance from the slab surface to the furthest inner extent of the hook indicates the thickness of surface layer that must be removed to eliminate the hook and the associated surface defects.

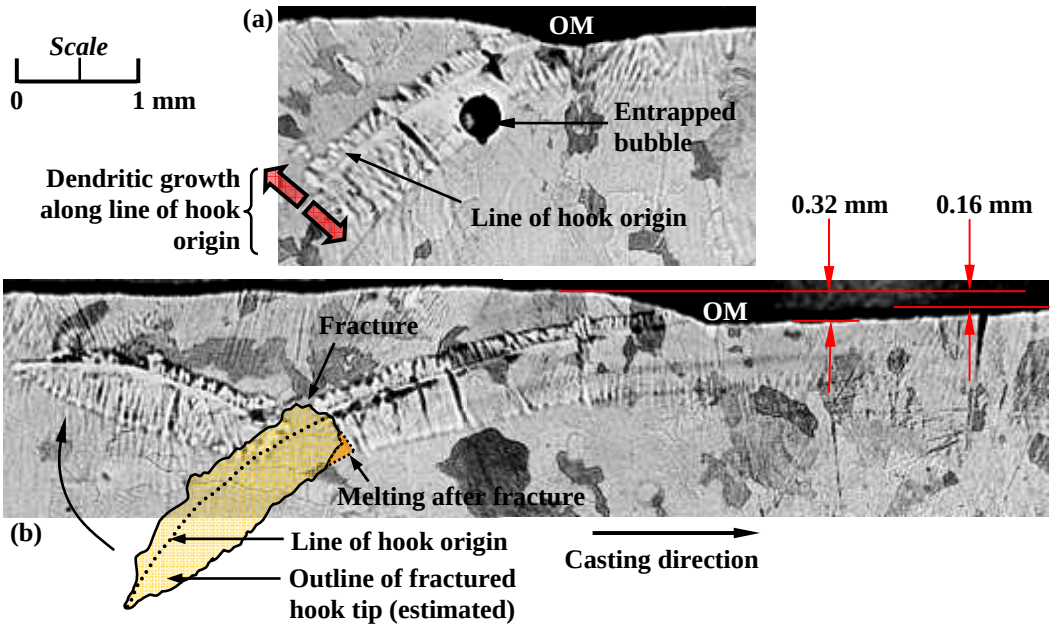

Figure 2 Hook features in ultra-low carbon steel samples: optical micrographs showing (a) entrapment of argon bubble by a hook-type oscillation mark (OM), and (b) a fractured hook tip.

Figure 2(b) shows a different curved hook located 35 mm (three oscillation marks away) from the hook in **Figure 2(a)**. This micrograph illustrates that a portion of the hook can be separated from the solidified meniscus. This indicates brittle fracture (hot tearing) of the fragile semi-solid hook that was likely caused by inertial forces of the molten steel acting during its overflow of the curved hook. This hypothesis is confirmed by the fact that the edges of the outline (estimated initial position) of the separated hook tip and the fractured hook in the figure align almost exactly. Just a small portion of the bottom edge of the hook tip is missing, which appears to have been melted away by the flowing liquid steel. The rest of the hook tip floated a short distance away and became entrapped in the solidifying shell growing above the hook. Usually, the fractured shell tip completely melts or is transported away, giving rise to the truncated end observed in most hooks, including the one in **Figure 2(a)**. This rare micrograph provides evidence that the characteristic truncated shape of most hooks is due to the breaking off of a longer, solidified meniscus.

The etched hook sample in **Figure 3** clearly reveals dendrites originating from several different nucleation sites located on or near the frozen meniscus (*i.e.* line of hook origin). Some dendrites grew away from the mold wall. Others grew into the liquid overflow region towards the mold wall, stopped growing and coarsened. The rest of the overflowed region solidified later, producing a finer structure, as heat was rapidly removed into the mold wall. A group of dendrites growing towards the molten steel abruptly changed direction near the truncated edge, in contrast to the uninterrupted growth in the same direction nearer to the base of the hook. This observation suggests that the truncated hook tip moved when liquid steel overflowed. If meniscus solidification and overflow usually occurs during the negative strip period[26, 27], it is proposed that the positive pressure in the flux channel can break and move the hook tip .

Orientation of grains near the hook region

Figure 4 shows an EBSD map of crystallographic orientations (left) obtained from an area near the line of hook origin on the slab sample shown in **Figure 2(a)**. The location of this area relative to the hook is indicated on the right. The relative orientation of several grains near the line of hook origin was found by combining the results of misorientation plots along 4 different lines (such as, "a-b" indicated in the figure) running across the microstructure. The misorientations of these grains ("B" through "F") are indicated on the map, relative to the largest grain ("A"). It can be clearly seen that the grains below the solid black line have different orientations than the grains above this line, which is a long grain boundary. The SEM image clearly shows that this line is indeed also a short segment

of the line of hook origin. The drastic difference in relative grain orientations suggests that solidification above and below the line of hook origin occurred at different times during the oscillation cycle. First, the lower region solidified while the interface (meniscus) was covered with mold flux, and then the upper side solidified during subsequent liquid steel overflow. This provides micrographic evidence for the overflow mechanism of hook formation.

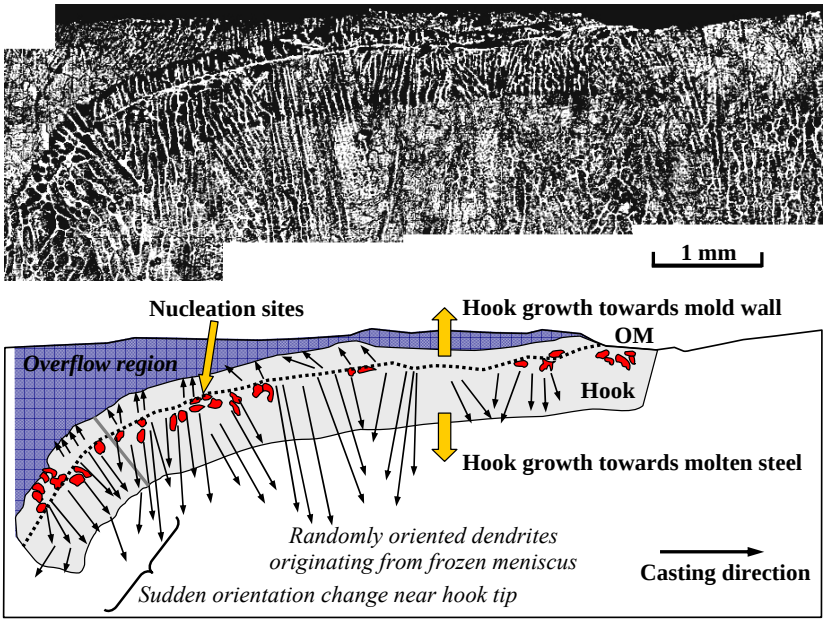

Figure 3 Optical micrograph of an ultra-low carbon steel sample showing unidirectional growth of dendrites originating from nucleation sites located at the line of hook origin (or frozen meniscus).

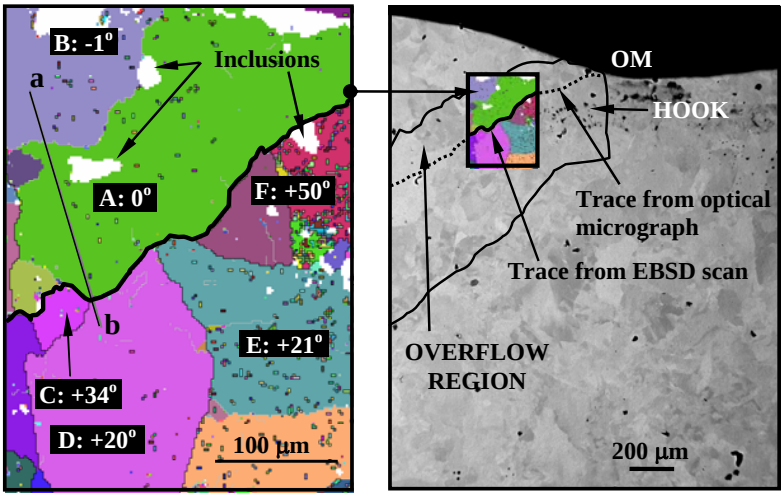

Figure 4 Electron Back Scatter Diffraction (EBSD) map of grain misorientation measured near the hook shown in Figure 2(a), and far-away view (EBS image) showing location relative to line of hook origin.

Elemental analysis of the hook region

Local composition traces were found using EDXS at two regions along the line of hook origin, indicated in **Figure 5**. Traces of fluorine and calcium were detected at areas "A" and "B", respectively. These elements are absent in the steel grade being investigated but are present in the mold powder. The appearance of these foreign elements along the line of hook origin suggests that some molten flux was retained by the δ-ferrite dendrites growing along the frozen meniscus, prior to liquid steel overflow. Clearly, some mold flux was entrapped by the overflow of liquid steel over the line of hook origin as solidification proceeded rapidly towards the mold wall. The authors believe that the surfactant used in the etching reagent preferentially reacted with the elements present in the mold powder that penetrated between the dendrites, and this enabled the shape of the hooks to be revealed by optical microscopy.

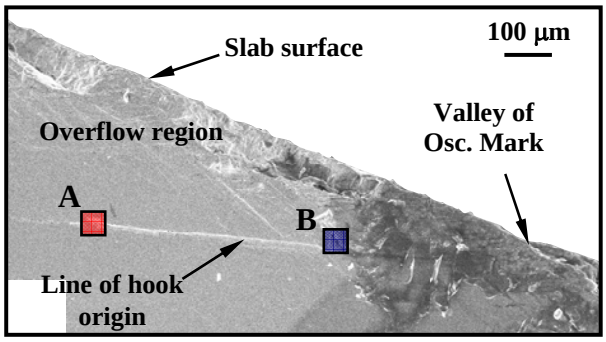

Element	Area A (wt %)	Area B (wt %)
C	5.65	16.6
S	0.22	---
Mn	0.68	---
F	0.81	---
O	---	47.16
Ca	---	33.11
Fe	Bal.	Bal.

Figure 5 Energy Dispersive X-ray Spectroscopy (EDXS) analysis at two locations on the line of hook origin shown on the SEM image reveals traces of fluorine & calcium oxide, which are present in the mold powder but not in the ultra-low carbon steel.

FINITE ELEMENT MODELING METHODOLOGY

The finite element model simulates the effect of level fluctuations on the thermo-mechanical behavior of a solidifying ultra-low carbon steel shell, as it moves down the 230-mm thick parallel mold at a casting speed of 23.33 mm/s (1.4 m/min). The liquidus and solidus temperatures of this steel grade are 1533 °C and 1517 °C, respectively. The mold oscillation frequency is 2.58 Hz (155 cpm) and the stroke is 6.34 mm. These parameters are typical of those used when the samples were cast. **Figure 5(a)** shows the computational domain, which is a 3 mm x 30 mm longitudinal slice along the centerline of the wide face (1300-mm in length) near the meniscus.

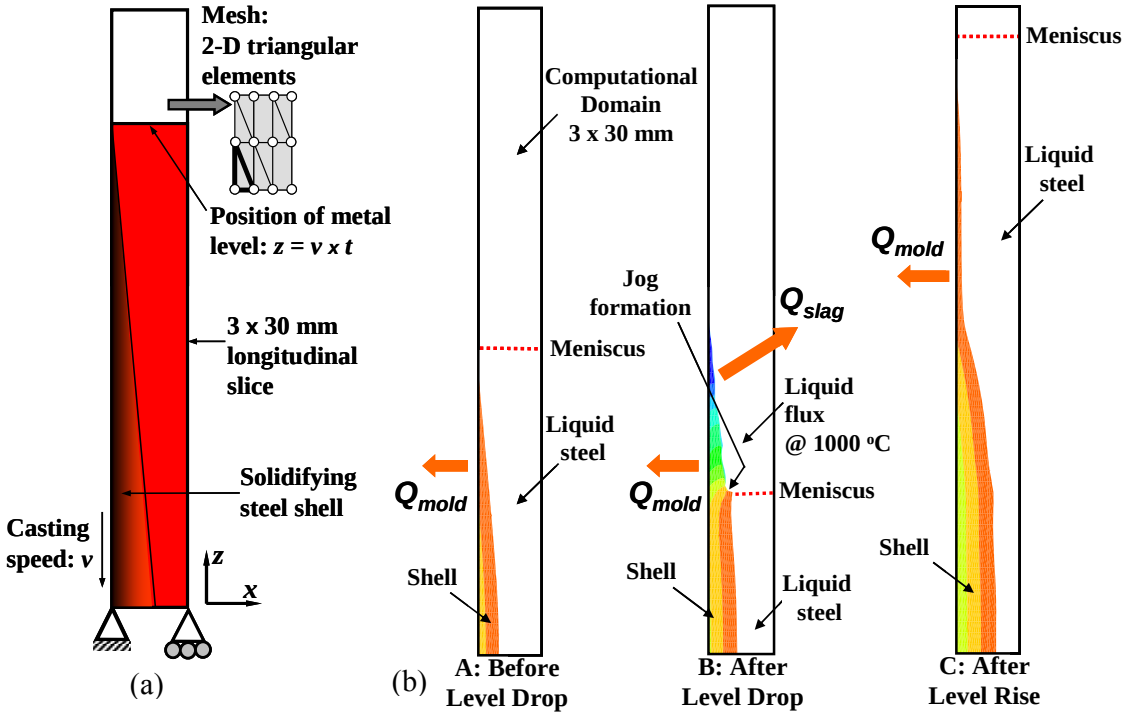

Figure 5 (a) Computational domain and mechanical boundary conditions used in CON2D for predicting shell distortion due to a sudden level fluctuation, and (b) thermal boundary conditions for the three different stages of the event.

The longitudinal slice enters the mold and moves downwards at the casting speed. Solidification proceeds from the left edge of the domain. At any time t, the metal level (ignoring meniscus curvature) is located just above the shell tip at $z = v \times t$ mm (see **Figure 5(a)**). Then, a sudden drop in metal level (by Δh mm) at $t_{drop} = 0.69$ s is imposed, exposing the inner edge of the shell to the liquid flux layer that floats above the liquid steel. Finally, a subsequent level rise occurs at $t_{rise} = 1.09$ s. The duration of the level fluctuation, $\Delta t = 0.4$ s corresponds to an oscillation cycle, or a chaotic wave generated by the turbulent flow. **Figures 6(a)** and **(b)** track the metal level changes in moving and stationary frames of reference, respectively, which are used to simulate a single level fluctuation event.

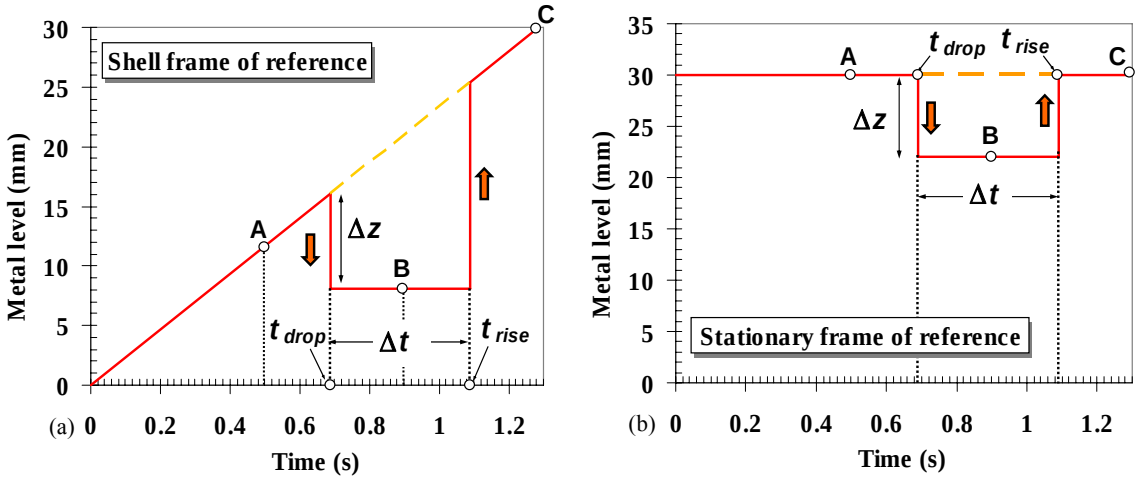

Figure 6 Metal level position in the computation domain during a level fluctuation event shown in two frames of reference: (a) moving (attached to shell) and (b) stationary. Three instants during the level fluctuation are shown – A: before level drop, B: after level drop, and C: after level rise. *Legend:* — *with &* - - *without level fluctuation.*

The heat flow model solves the 2-D transient energy equation, using a fixed Lagrangian grid of 3-node triangles. Temperature-dependent thermal conductivity and enthalpy functions are used to incorporate the effects of solidification and solid-state phase transformation on the heat flow across the domain[23]. A non-equilibrium micro-segregation model incorporating the effects of several alloying elements is used to calculate the liquidus, solidus, and peritectic temperatures, and phase fractions[28]. Within each time step, temperatures are first computed by the heat transfer model. After interpolating the thermal loads onto a fixed-grid finite element mesh of 6-node triangles, the stress model then solves for stresses, strains, and displacements. The effects of stiffness and volume changes during solidification are incorporated through temperature-dependent Young's modulus and thermal linear expansion functions[23].

To discretize the computational domain, a grid of 31 nodes x 61 nodes (mesh resolution: 0.1 mm x 0.5 mm) was selected based on a sensitivity analysis conducted for a normal solidification case without any level fluctuation. The domain is initially assumed to contain stress free liquid at the uniform pour temperature of 1565 °C. Solidification is achieved by imposing a convection boundary condition on the left edge of the domain that contacts the water-cooled mold. Zero heat flux is assumed on all other edges, including that portion of the edge above the metal level. Thus, non-uniform fluid flow effects in the meniscus region are not taken into account.

Heat flux to the mold (Q_{mold} in W/m^2) (or primary cooling) before the level drop (event "A" in **Figure 5(b)**) is given by:

$$Q_{mold} = 0 \qquad \text{for } t > 0 \text{ s}, x = 0 \text{ mm}, \& z > z = v \times t \qquad (1)$$

$$Q_{mold} = h_{mold}\,(T - T_{mold}) \qquad \text{for } t > 0 \text{ s}, x = 0 \text{ mm}, \& z \le z = v \times t \qquad (2)$$

The mold wall temperature T_{mold} is fixed at 250 °C, and the heat transfer coefficient, h_{mold} is 4000 W/m^2-K, which corresponds to a heat flux of ~5.0 MW/m^2 near the meniscus.

At time, t_{drop} = 0.69 s, the level drops suddenly by ~16 mm (event "B" in **Figure 5(b)**) for a duration of 0.4 s. During this time, liquid mold flux is drawn into the domain to replace the liquid steel. This is accomplished by changing the thermal properties of the liquid nodes (beyond the solidification front) to that of liquid flux and changing their temperatures to the constant T_{flux} = 1000 °C. Heat is then extracted from the exposed inner surface of the solid shell, by imposing the following boundary condition on the solidus isotherm at the time of the level drop:

$$Q_{flux} = h_{flux}\,(T - T_{flux}) \qquad \text{for } t_{drop} \le t \le t_{rise} \text{ with } h_{flux} = 1500 \text{ W/m}^2\text{-K} \qquad (3)$$

Finally, the level is raised again at time, t_{rise} = 1.09 s (event "C" in **Figure 5(b)**), by restoring the liquid elements to their liquid steel properties and initial temperature, and allowing solidification to proceed normally. Since the level is restored above the shell tip, the model simulates meniscus overflow, which is an important event associated with oscillation mark formation[2, 12, 13]. The model ignores non-uniform dissipation of superheat and nucleation under-cooling near the meniscus, so the possibility of meniscus solidification is not considered.

The mechanical boundary conditions imposed on the domain are indicated in **Figure 5(a)**. The shell tip is assumed to be attached to the rigid lower portion of the solidifying shell (below the model domain), but it is free to move away or towards the mold so that the

formation of an oscillation mark or a surface depression can be simulated. This condition is accomplished by preventing movement of the bottom edge of the domain in the casting direction, and completely constraining the bottom-left node. Mold friction and pressure forces imposed on the shell by the liquid flux and slag rim (~1 kPa), and ferrostatic pressure (~0.002 MPa at the bottom of the domain) are ignored. Although these effects are important to meniscus shape, they are believed to be too small to affect the distortion of the solid shell caused by thermal stress. The longitudinal slice is assumed to remain planar as it moves down the mold; thus, the wide and thin shell is in a stress state of generalized plane strain. This condition allows the 2-D model to reasonably estimate the complete 3-D stress state for the domain under consideration.

Model predictions

Figure 7 shows the evolution of shell shape and distortion at three different times during a level fluctuation event (refer to **Figure 6**) computed by the model as the domain travels down the mold length at the casting speed. The stresses across the thickness (σ_{xx}) and in the transverse direction (σ_{yy}) are very small (< ± 1.0 MPa) for a shell length of ~16 mm owing to rapid creep relaxation and low elastic modulus at the high temperatures experienced. Before the level drops, solidification produces a classic solid shell with parabolic shape and a thermal gradient quickly develops inside. The surface cools faster than the interior, causing the shell tip to bend towards the mold (by ~0.02 mm) and axial tensile stress to develop near the surface.

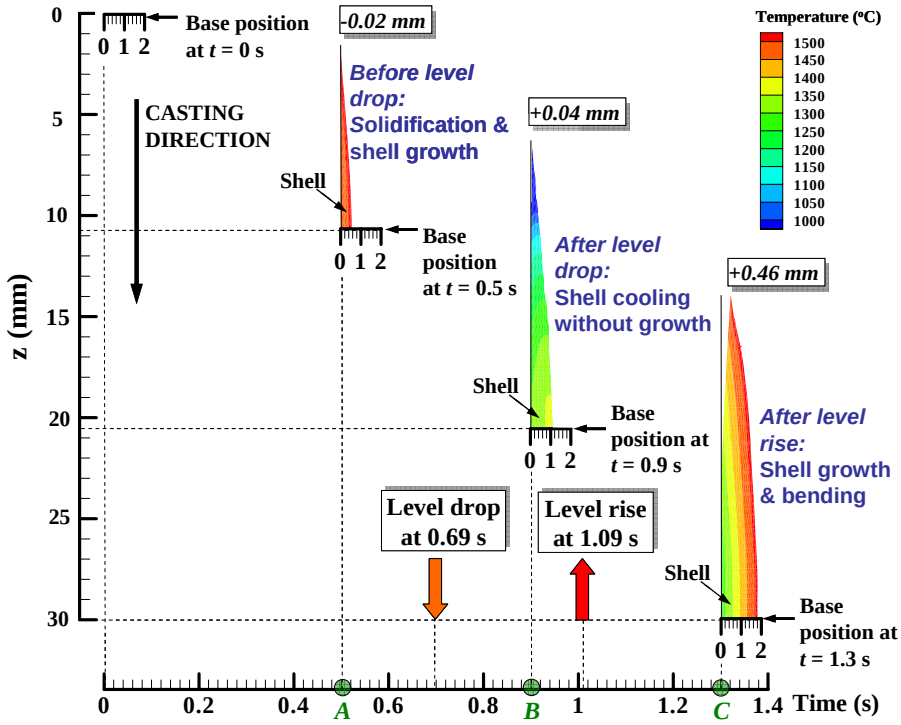

Figure 7 Evolution of temperature and shell tip deformation during a level fluctuation event. Contour plots are shown at three representative times : (A) 0.19 s before the level drops, (B) 0.21 s after the level drops, and (C) 0.21 s after the level rises again.

After the level drops, exposing the shell to mold flux, the shell temperature decreases rapidly (~200 °C in 0.19 s) because the mold extracts sensible heat from the thin shell very quickly in the absence of heat supply from the liquid steel. The thermal gradient inside the shell also disappears, causing the shell interior to contract more than its exterior. Thus, a relatively large compressive stress develops at the surface, and the shell tip bends away from the mold wall (by ~0.04 mm). Suddenly raising the liquid level back up to the shell tip, is predicted to rapidly increase the shell temperature, shell thickness, and distortion. Liquid steel comes in direct contact with the colder shell, and a new skin grows over the older shell. Restoring the high temperature gradient across the entire thickness tends to cause the older shell to expand. Because this is constrained by the newly-solidified layer, the net effect is to bend the shell tip substantially towards the liquid steel, (up to 0.46 mm within 0.21 s time span).

Although a level drop of ~16 mm was chosen in the previous case to demonstrate the thermo-mechanical behavior of the shell during a level fluctuation event, a level drop of this magnitude occurs only rarely in an industrial casting machine, and is normally within ±10 mm[29]. Thus, the model was utilized to compute the shell shapes and distortions for smaller level fluctuations keeping the duration constant at 0.4 s. The results are summarized in **Figure 8(a)**, which indicates that shell tip distortion is almost negligible for fluctuations below ~5 mm. An irregularity in the profile of the inner shell edge was always observed near the location where the liquid level stays stationary for 0.4 s during the level drop event. Ordinary solidification below this location increases the shell thickness, in contrast to the shell edge above this location, which cannot grow, due to the absence of liquid steel. Thus, the formation of a "jog"

(refer to **Figure 5(b)**) is predicted by the model, similar to the one observed in the plant sample[30] in **Figure 8(b)**. This jog is smoothened out after the liquid level rise.

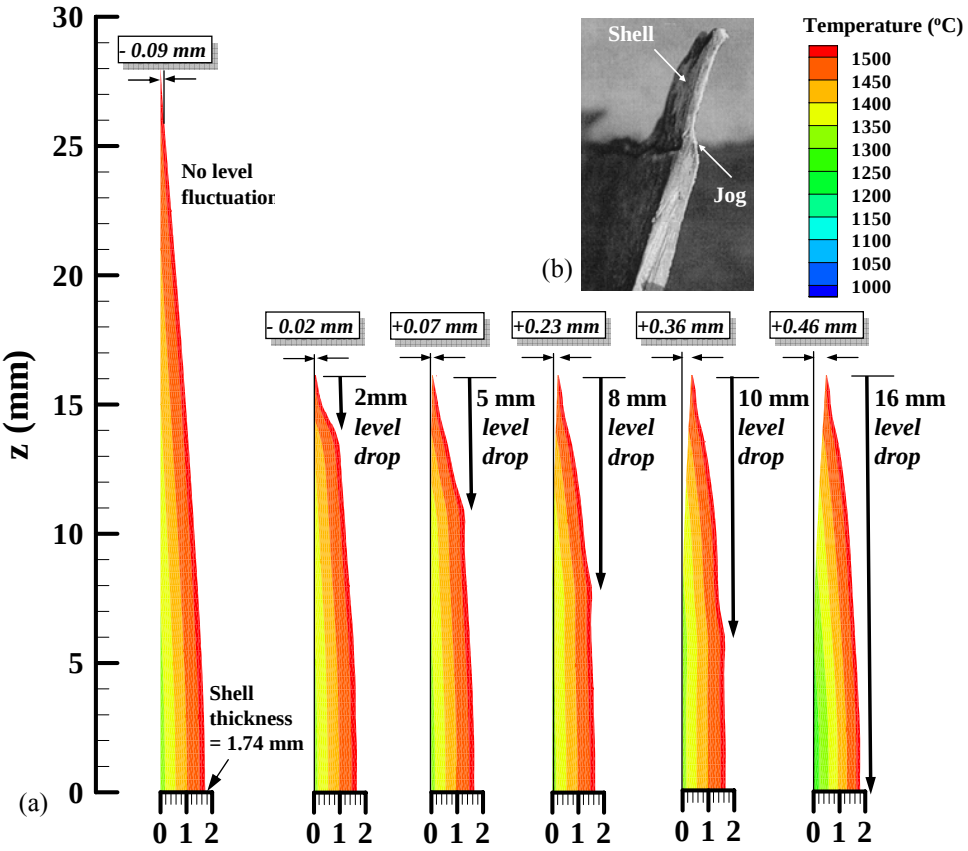

Figure 8 (a) Comparison of temperature and shell distortion predicted after different magnitudes of level drop. (b) Jog formation on the inside edge of the shell observed by Fredriksson and Elsberg[30] in a breakout shell.

IMPLICATIONS FOR HOOK & OSCILLATION MARK FORMATION

Important new insights into hook formation are gained by comparing the thermal stress model results with Bikerman's equation for meniscus shape and the metallographic analysis of hooks from the slab samples. **Figure 9(a)** shows the lines of hook origin (dotted lines) observed in successive hooks on two ~100-mm long steel slab samples. They are compared with the equilibrium shape of the meniscus from Bikerman's equation,[30] determined solely by balancing the ferrostatic pressure forces on the interface with the surface tension forces. The calculation here assumed a surface tension of 1.6 N/m, corresponding to the sulfur content of 0.01 % for this steel grade[30], and the steel density of 7000 kg/m^3 at 1560 °C[31]. A reasonable match between the hook shapes and the shape predicted by Bikerman's equation confirms that *curved hooks* are indeed initiated by meniscus solidification in ultra-low carbon steel slabs. This figure also shows that these hooks are curved much more than the maximum curvature expected from thermal distortion of the initial shell, even for a level fluctuation of 16 mm for 0.4 s (obtained from **Figure 8(a)**). Thus, thermal stresses likely play a much smaller role, perhaps increasing the hook curvature slightly due to thermal expansion of the line of hook origin during meniscus overflow. The curved bottom portion of straight hooks (located close to the surface) may be formed solely by the thermal distortion effect after level fluctuations, however. This role of thermal stress in the formation of *straight hooks* would explain the observed increase in the occurrence of straight hooks with increasing level fluctuations during the casting process, which is presented in **Figure 9(b)**.

The measurements in Fig. 9(a) show a wide variation of the depth and length of curved hooks, indicating that hook formation is a complex event dictated by the time-dependent meniscus shape as it freezes over the initial shell tip. This observation suggests that the shape of the meniscus can be significantly altered during the casting process. This can be attributed to: (i) periodic pressure forces generated in the flux channel by the oscillating mold[12, 32], and (ii) sudden localized metal level fluctuations initiated by chaotic turbulent motion in the molten pool or by abrupt changes in fluid flow conditions. These phenomena are investigated elsewhere.[33]

The results of this work reveal new insights about how hooks form in ultra-low carbon steel:

(i) Formation of curved hooks starts by meniscus solidification. The shape of the meniscus at this instant dictates the curvature of the line of hook origin. Recent work has established that this event usually occurs near the beginning of the negative strip period[27]. This is schematically illustrated in **Figure 10 (a)**. In contrast, it is likely that straight hooks are initiated by thermal distortion of the shell tip, thus resulting in a smaller hook depth.
(ii) The hook thickness below the line of hook origin is created by dendritic growth towards the molten steel, originating from nucleation sites along the under-cooled meniscus (eventual line of hook origin).
(iii) Some of the molten flux contacts the meniscus and penetrates between the dendrites of the solidifying hook[25], where it is retained and revealed during etching.
(iv) The meniscus subsequently overflows the line of hook origin during the negative strip time[27] as soon as inertial forces instantaneously exceed surface tension forces, as shown in **Figure 10(b)**. Dendrites quickly grow above the line of hook origin towards the mold wall into the overflowed liquid. The growth eventually stops as the meniscus region gains superheat. The hook edges are established as the dendrites coarsen due to the long local solidification time[27]. This event explains the sharp drop in the distance between solidified shell and mold wall during the negative strip time measured by Tsutsumi *et al.*[34] while observing oscillation marks and mold powder infiltration in a Sn-Pb alloy (metal) and stearic acid (flux) system. It also explains the rapid rise of mold heat flux throughout the negative strip time, observed during experiments by Badri *et al.*[26]
(v) The heavier liquid steel displaces liquid mold flux as it overflows. It also melts through some of the solid mold flux layer, bringing liquid steel closer to the mold wall. This explains the eventual outward bulge usually observed above every oscillation mark and line of hook origin. For example, in **Figure 2(b)**, the slab surface above the oscillation mark extends d = 0.32 mm beyond the oscillation mark root and 0.16 mm beyond the slab surface below the oscillation mark. This indicates that the overflow caused ~0.16 mm of the flux layer thickness to re-melt.
(vi) The heat transfer rate increases during this time because it is controlled by the gradually decreasing thickness of the mold flux layer that separates the mold and the molten steel. The heat transfer rate is largest while the steel is still liquid, before solidification produces a surface roughness and solid layer that slows down heat transfer.
(vii) Molten flux is retained along the line of hook origin, which is revealed by EDS and EPMA analysis. Some flux is also retained within the overflowed region.
(viii) The line of hook origin persists as grain boundaries in the final microstructure[25], despite the occurrence of two separate phase transformations, as revealed by the EBSD analysis. Grains above and below the line of hook origin have distinctly different crystallographic orientations due to the temporal separation between meniscus freezing and liquid overflow.
(ix) The final shape of the hook is completed as the hook tip fractures off and is carried away, as shown in **Figure 10(c)**.
(x) The overflow region solidifies forming the oscillation mark during the positive strip time. The extent of penetration of liquid steel into the flux channel determines the final shape of the upper side of the oscillation mark. The extra volume of flux entrapped in the oscillation mark during its formation at this time explains the sudden rise in tracer velocity measured in the stearic acid flux channel between the mold wall and shell during the positive strip time[34]. The hook protruding from the solidifying shell captures inclusions and bubbles in the liquid steel until the shell finally solidifies past the hook. These events are illustrated in **Figure 10(d)**.

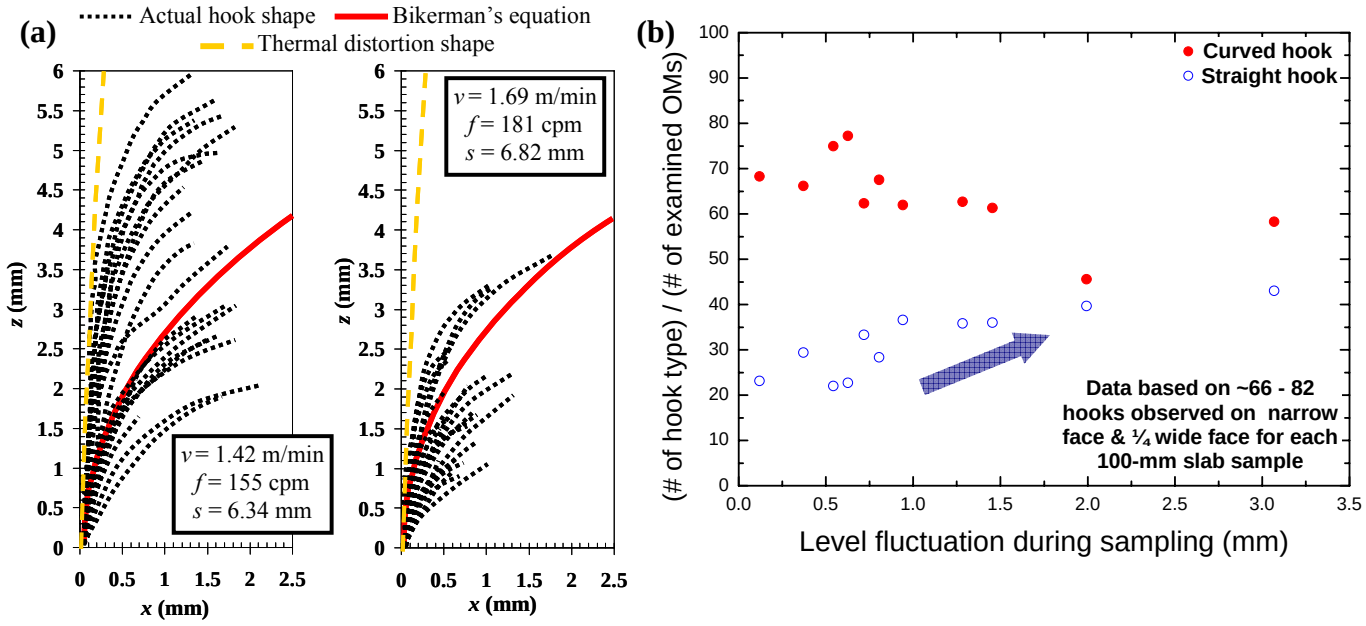

Figure 9 (a) Line of hook origin for successive hooks on slab samples cast under two different conditions. Comparison with Bikerman's equation, and predicted shell shape after a level fluctuation is also included. (b) Plant data showing that occurrence of surface hooks increases with an increase in metal level fluctuation recorded during the casting process.

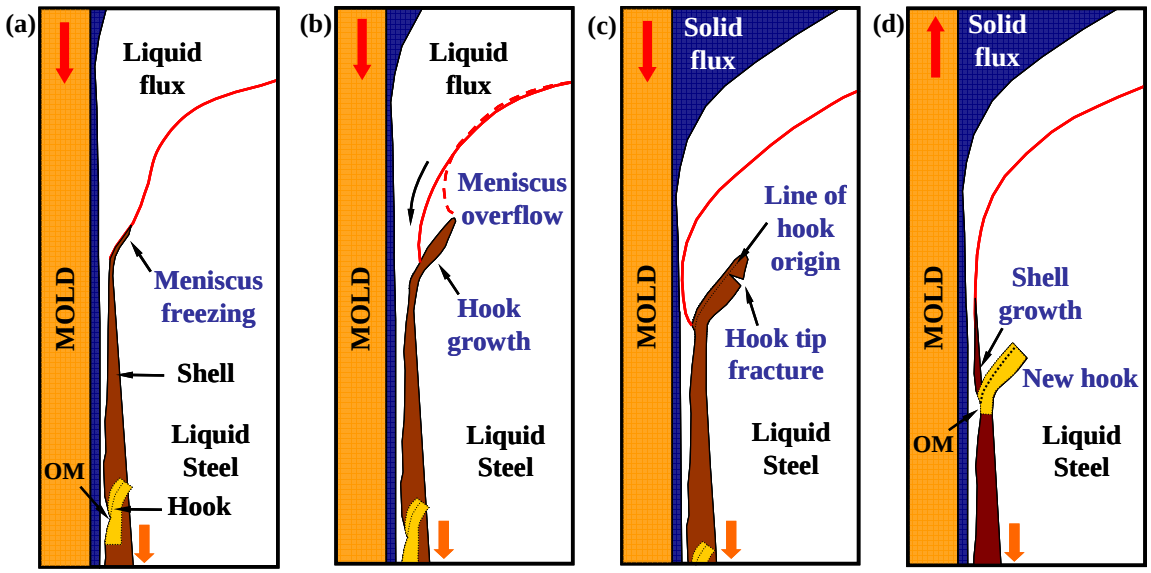

Figure 10 Schematics illustrating formation of curved hook in an ultra-low carbon steel slab by meniscus solidification and subsequent liquid steel overflow. Oscillation marks are formed by normal steel shell growth after overflow.

CONCLUSIONS

The sub-surface microstructure of continuous-cast ultra-low carbon steel slabs has been examined using both optical microscopy and scanning electron microscopy using EBSD and EDX techniques. Careful selection of an etching reagent allowed the dendrites forming the hook to be clearly distinguished from the rest of the microstructure using optical microscopy. Measured shapes of the line of hook origin matched reasonably well with Bikerman's equation for meniscus shape. This confirms that periodic meniscus solidification during the continuous casting process causes curved hook formation.

Grain orientation measurements and elemental maps confirm that dendritic growth above the line of hook origin occurs after meniscus overflow over the solidified hook, which also entraps liquid mold flux and persists in the final microstructure. A hook tip that was fractured off, likely during liquid steel overflow, was revealed in the solidified microstructure, and explains the characteristic truncated shape of hook. Thus, the shape and size of hooks and oscillation marks are determined by two crucial events: (i) the curvature of the line of hook origin as dictated by the instantaneous shape of the meniscus during its solidification, and (ii) the shape of the upper side of the oscillation mark, as dictated by the extent of liquid steel overflow.

A 2-D transient finite-element model of thermomechanical behavior during solidification has been successfully applied to reasonably predict shell shape and distortion due to a sudden level fluctuation event for ultra-low carbon steel slabs. A sudden level drop causes the shell tip to bend away from the mold. Subsequent rise in liquid level causes further shell bending. Shell distortion is small for rapid level drops less than ±5 mm; however, for larger drops, such as 16 mm for 0.4 s, shell bending can create a gap 0.46 mm deep. Although shell distortion alone cannot produce curved hooks and their associated oscillation marks, shallower straight hooks may be created by this mechanism. In particular, ultra-low carbon steels and peritectic steels, which tend to produce a stronger initial shell that cannot be flattened by ferrostatic pressure, are expected to suffer more from thermal distortion effects.

Hooks and their associated surface defects can be decreased by controlling the phenomena that cause them. Promising strategies consistent with the mechanism in this work include: preventing meniscus freezing (by raising superheat delivery to the meniscus region or by introducing nucleation agents), decreasing level fluctuations (both short and long term), minimizing the solid slag rim, optimizing mold flux properties, and minimizing the transients associated with mold oscillation (by increasing frequency and decreasing stroke). Much further work is needed to quantify these conditions.

ACKNOWLEDGEMENTS

The authors wish to thank the Natural Sciences and Engineering Research Council of Canada, the National Science Foundation (Grant DMI-05-28668) and the Continuous Casting Consortium at the University of Illinois at Urbana-Champaign for support of this project.

REFERENCES

1) J. K. Brimacombe and K. Sorimachi: *Metallurgical Transactions B*, (1977), **8B**, 489.
2) E. Takeuchi and J. K. Brimacombe: *Met. Trans B*, (1984), **15B** (Sept), 493.

3) E. Takeuchi and J. K. Brimacombe: *Met. Trans B*, (1985), **16B** (Sept), 605.
4) H. Yamamura, Y. Mizukami and K. Misawa: *ISIJ International (Japan)*, (1996), **36** (Suppl. Science and Technology of Steelmaking), 223.
5) M. Suzuki: *CAMP-ISIJ*, (1998), **11**, 42.
6) S. Harada, S. Tanaka, H. Misumi, S. Mizoguchi and J. Horiguchi: *ISIJ International*, (1990), **30(4)**, 310.
7) H.-J. Shin, G.-G. Lee, W.-Y. Choi, S.-M. Kang, J.-H. Park, S.-H. Kim and B. G. Thomas: *AISTech 2004 Iron & Steel Technology Conference Proceedings - Vol. II*, The Association for Iron & Steel Technology (AIST), Warrendale, PA, Nashville, TN, (2004), 1157-1170.
8) H.-J. Shin, B. G. Thomas, G.-G. Lee, J.-M. Park, C.-H. Lee and S.-H. Kim: *MS&T 2004 Conference Proceedings*, The Association for Iron and Steel Technology (AIST) and TMS, Warrendale, PA, New Orleans, LA, (2004), 11-26.
9) L. Reda, C. Genzano and J. Madias: *2001 Steelmaking Conference*, D.L. Kanagy, eds., Iron and Steel Society, Warrendale, PA, Baltimore, U.S.A., (2001)**, 84**, 771-780.
10) K. D. Schmidt, F. Friedel, K. Imlau, W. Jager and K. T. Muller: *Steel Research International*, (2003), **74(11-12)**, 659.
11) J.-P. Birat, M. Larrecq, J.-Y. Lamant and J. Petegnief: *Steelmaking Conference Proceedings*, (1991), **74**, 39.
12) T. Emi, H. Nakato, Y. Iida, K. Emoto, R. Tachibana, T. Imai and H. Bada: *Proceedings of National Open Hearth and Basic Oxygen Steel Conference*, (1978), **61**, 350.
13) K. Schwerdtfeger and H. Sha: *Metall. Mater. Trans. B*, (2000), **31B** (4), 813.
14) I. G. Saucedo, in Steelmaking Conf. Proc., **74**, Iron and Steel Society, Washington, D.C., (1991), 79-89.
15) K. Bo, G. Cheng, J. Wu, P. Zhao and J. Wang: *Journal of University of Science and Technology Beijing*, (2000), **7(3)**, 189.
16) O. Putz, O. Breitfeld and S. Rodl: *Steel Research*, (2003), **74(11-12)**, 686.
17) E. S. Szekeres: *Iron and Steel Engineer (USA)*, (1996), **73** (7), 29.
18) R. Sato: *Proceedings of National Open Hearth and Basic Oxygen Steel Conference*, AIME, Warrendale, PA, Detroit, MI, (1979)**, 62**, 48-67.
19) J. Savage and W. H. Pritchard: *J. Iron Steel Inst.*, (1954), **178**, 269.
20) J. L. Brendzy, I. A. Bakshi, I. V. Samarasekera and J. K. Brimacombe: *Ironmaking and Steelmaking*, (1993), **20 (1)**, 63.
21) B. G. Thomas and H. Zhu: *Proceedings of JIM/TMS Solidification Science and Processing Conference*, TMS, Warrendale, PA, Honolulu, Hawaii, (1995), 197-208.
22) A. Yamauchi, S. Itoyama, Y. Kishimoto, H. Tozawa and K. Sorimachi: *ISIJ International*, (2002), **42(10)**, 1094.
23) C. Li: Ph. D. Thesis, University of Illinois at Urbana-Champaign, Urbana IL, (2004).
24) G. F. V. Voort: *Materials Characterization*, (1995), **35(2)**, 135.
25) J. Sengupta, H. J. Shin, B. G. Thomas and S. H. Kim. Micrograph evidence of meniscus solidification and sub-surface microstructure evolution in continuous-cast ultra-low carbon steels. Acta Materialia. (2006), **54**(4), 1165.
26) A. B. Badri and A. W. Cramb: *85th Steelmaking Conference*, Iron and Steel Society, Nashville, TN, USA, (2002)**, 85**, 65-76.
27) J. Sengupta, B. G. Thomas, H. J. Shin and S. H. Kim. A New Mechanism of Hook Formation during Continuous Casting of Ultra-low Carbon Steel Slabs *Metall. and Mater. Trans. A*, (2006), in press.
28) Y. Meng and B. G. Thomas: *Metallurgical Transactions B*, (2003), **34B**, 685.
29) W. Lai, M. Milone and I. Samarasekera, in Steelmaking Conf. Proc., **83**, ISS, Warrendale, PA, Pittsburgh, PA, (2000), 461-476.
30) S. K. Kim, Y. D. Lee, K. Hansson and H. Fredriksson: *ISIJ Internat.*, (2002), **42** (5), 512.
31) I. Jimbo and A. W. Cramb: *Iron & Steelmaker*, (1993), **20(6)**, 55.
32) S. Takeuchi, Y. Miki, S. Itoyama, K. Kobayashi, K. Sorimachi and T. Sakuraya: *Steelmaking Conference Proceedings*, (1991), 37.
33) C. Ojeda, J. Sengupta, B.G. Thomas, J. Barco, and J.L. Arana, *AISTech 2006*, Cleveland, OH, May 1-4, 2006. (2006).
34) K. Tsutsumi, J. Ohtake and M. Hino: *ISIJ International*, (2000), **40**, 601.